

# A Comparative Study of Different Level Interpolations for Improving Spatial Resolution in Diffusion Tensor Imaging

Feng Yang, Yue-Min Zhu, Jian-Hua Luo, Marc Robini, Jie Liu, and Pierre Croisille

**Abstract**—This paper studies and evaluates the feasibility and the performance of different level interpolations for improving spatial resolution of diffusion tensor magnetic resonance imaging (DT-MRI or DTI). In particular, the following techniques are investigated: anisotropic interpolation operating on scalar gray-level images, log-Euclidean interpolation method, and the quaternion interpolation method, which operate on diffusion tensor fields. The performance is evaluated both qualitatively and quantitatively using criteria such as tensor determinant, fractional anisotropy (FA), mean diffusivity (MD), fiber length, etc. We conclude that tensor field interpolations allow avoiding undesirable swelling effect in DTI, which is not the case with scalar gray-level interpolation, and that scalar gray-level image interpolation and log-Euclidean tensor field interpolation suffer from decrease in FA and MD, which may mislead the interpretation of the clinical parameters FA and MD. In contrast, the quaternion tensor field interpolation avoids such FA and MD decrease, which suggests its use for clinical applications.

**Index Terms**—Diffusion tensor imaging, diffusion-weighted (DW) image, fiber tractography, interpolation, magnetic resonance imaging (MRI), tensor field interpolation.

## I. INTRODUCTION

**D**IFFUSION tensor magnetic resonance imaging (DT-MRI or DTI) [1] has gained considerable attention and importance in recent years in the field of medical imaging and clinic researches. It provides a unique noninvasive *in vivo* imaging technique to get insights into the biologically and clinically relevant information by measuring the relative diffusion coefficient of water molecules in different directions. This information

includes parameters that help characterize the tissue composition, physical properties of tissue constituents, tissue microstructure and its architectural organization. In DTI, the ultimate quantity to be calculated for each voxel is not a scalar, but a tensor that describes local water diffusion and is expressed as a  $3 \times 3$  symmetric positive-definite matrix (in this study, we adopted the commonly used constraint of positive definiteness on a diffusion tensor, although the latter is, strictly speaking, symmetric positive semidefinite) [2]. However, due to technical limitations of MRI machines, DTI is sensitive to the difficult compromise between spatial resolution and noise or artifacts [3], and the data are often acquired with low resolution. To improve DTI data resolution, interpolation provides an interesting software solution. Interpolation in DTI can be dealt with at different levels. It can be performed at the level of diffusion-weighted (DW) gray-level images or at the level of tensor fields or still at the level of vector fields. Vector field level interpolations are desired when one aims at fiber structure or when only vector field information is available [4]–[7]. In contrast, DW gray-level image interpolation and tensor field interpolation provide more information such as fractional anisotropy (FA) and mean diffusivity (MD) parameters in addition to fiber orientation information. In the following, we focus on the interpolations at the level of DW gray-level images and tensor fields.

Although there exist only a few works on interpolation of DW images, such interpolation still remains basically an issue of scalar image interpolation. In this sense, this is a classical image processing problem for which a variety of methods exist [8], [9], such as nearest interpolation, linear interpolation, quadratic interpolation, B-spline interpolation, cubic interpolation, etc. The critical element of these interpolation techniques is the interpolation kernel, which distinguishes different interpolation techniques and determines their performance. Detailed comparisons of these methods are reported in [8] and [9] in terms of spatial and Fourier analysis, computational complexity, and error determinations. Based on the work of Lehmann *et al.* [8] and [9], the authors of [10] proposed an anisotropic interpolation for DT-MRI data, which is space-variant and can reduce noise without compromising the sharpness of boundaries. Other types of scalar image interpolation methods include variational [11], [12] and partial differential equation (PDE)-based [13] interpolations, which account for the local geometric structure of the image by efficiently reconstructing image boundaries.

In contrast to the interpolation of scalar images, the interpolation of diffusion tensor fields is a relatively new problem in the

Manuscript received April 9, 2013; revised December 16, 2013; accepted February 7, 2014. Date of publication February 19, 2014; date of current version June 30, 2014. This work was supported in part by the Fundamental Research Funds for the Central Universities under Grant 2013JBZ014, the French ANR under ANR-13-MONU-0009-01, the National Basic Research Program of China under Grant 61301002, Specialized Research Fund for the Doctoral Program of Higher Education under Grant 20130009120039, the University Funds for Talents under Grant 2012RC037, and the Chinese government funding under Grant 30970777.

F. Yang and J. Liu are with the School of Computer and Information Technology, Beijing Jiaotong University, Beijing 100044, China (e-mail: fengyang@bjtu.edu.cn; jliu@bjtu.edu.cn).

Y.-M. Zhu, M. Robini, and P. Croisille are with the CREATIS, CNRS UMR 5220, Inserm U1044, INSA Lyon, University of Lyon, Villeurbanne 69100, France (e-mail: zhu@creatis.insa-lyon.fr; robini@creatis.insa-lyon.fr; croisille@creatis.insa-lyon.fr).

J.-H. Luo is with the School of Aeronautics and Astronautics, Shanghai Jiao-tong University, Shanghai 200240, China (e-mail: jhluo@sjtu.edu.cn).

Color versions of one or more of the figures in this paper are available online at <http://ieeexplore.ieee.org>.

Digital Object Identifier 10.1109/JBHI.2014.2306937

field of image processing, and there are only a few interpolation techniques that are reported in the literature. Diffusion tensor interpolation operates directly on tensors. The most straightforward method for interpolating diffusion tensors is the Euclidean method that consists of interpolating each tensor component independently in Euclidean space [14]. However, tensor processing is difficult due to some limitations of standard Euclidean calculus. Diffusion tensors do not form a vector space since they are symmetric positive-definite matrices whose space is restricted to a convex half-cone [15]. Therefore, special care must be taken in order not to reach the boundaries of the nonlinear tensor space, which lead to null or negative eigenvalues. On the purpose of maintaining the symmetric positive-definite property, anisotropic interpolation [14], PDE interpolation [16], tensor spline interpolation [17], and Cholesky factorization-based interpolation [18] were proposed for diffusion tensors. However, these methods exhibit the tensor swelling effect, which reflects the fact that interpolating two tensors yields a tensor with a determinant larger than either of the original tensors [15], [19], still due to the limitations of Euclidean space. To simultaneously eliminate the swelling effect and preserve the positive-definiteness property of diffusion tensor, the authors of [20] presented a geodesic interpolation and a rotational interpolation in the Riemannian matrix sense, while in [19] the PDEs were studied within the affine-invariant framework for applications such as diffusion tensor field interpolation. Interpolation methods in Riemannian space are computationally expensive because of intensive use of logarithms, exponentials, inverses, and square roots on matrices. To overcome the computational limitation of Riemannian space, log-Euclidean metric [15] was proposed that performs classical Euclidean computations after taking the logarithm of the tensor matrix, while being a close approximation of the Riemannian method. Log-Euclidean interpolation is rigorous in keeping the determinant of tensor vary monotonically and preserving symmetric positive-definite property. In [21] and [22], a class of so-called interpolation paths for tensors was proposed, called geodesic-loxodromes, in order to preserve clinically important tensor attributes and measure the difference in tensor shape and orientation. The geodesic-loxodromes method can monotonically interpolate some tensor attributes such as FA or MD. But it cannot avoid the swelling effect. To simultaneously avoid the swelling effect and decrease in FA and MD tensor attributes, a feature-based interpolation method was proposed that consists of first decomposing a diffusion tensor into eigenvalues and orientation, then representing the tensor orientation using quaternions [23], and finally interpolating the three eigenvalues in logarithm and the quaternion.

Since DTI yields systematically both scalar DW images and tensor fields, a question arises whether interpolation should be performed at the level of DW images or at that of tensor fields. A preliminary work on such comparative study of different level interpolations in DTI is reported in [24]. The aim of this work is to give a systematic, quantitative, and detailed study about the interpolations at different levels and to evaluate the feasibility and the performance of different interpolation techniques. To do that, we propose to consider the interpolation at different levels. For the interpolation of scalar DW gray-level images, we

focus on the anisotropic interpolation method [14], and for that of diffusion tensor fields, we use log-Euclidean interpolation method [15] and the quaternion interpolation method [23]. The evaluation is performed both qualitatively and quantitatively in terms of tensor determinant, FA, MD, and fiber length.

## II. STRATEGIES OF INTERPOLATION FOR DTI DATA

The raw data provided by DTI are the gray-level DW images, from which tensor data are computed. So, a straightforward way of interpolating DTI data would consist in interpolating the DW images, from which the interpolated tensor data can be consequently obtained. Meanwhile, we can also directly interpolate the diffusion tensor fields. Note that interpolation can also be achieved at the level of tensor parameter maps such as FA or MD, depending on the application in question. However, it is DW images or tensors that contain the most complete information, based on which all other parameters (FA, MD, vector field, fiber angles, fiber tractography, etc.) used in practices can be calculated. That has led us to emphasize the DW image and diffusion tensor field interpolations.

### A. DW Image Interpolation

In DTI, the acquired DW images are used to calculate diffusion tensors according to the Stejskal–Tanner diffusion equations [25]:  $S_i = S_0 \exp(-b\mathbf{g}_i \mathbf{D} \mathbf{g}_i^T)$ , where  $S_0$  is the magnetic resonance measurement without diffusion sensitization,  $S_i, i = 1, \dots, N$  ( $N$  is the number of gradient directions and must be greater than or equal to 6), is the image intensity measured after the application of the  $i$ th diffusion-sensitizing gradient,  $\mathbf{g}_i$  is the diffusion encoding gradient direction associated with  $S_i$ ,  $b$  is the diffusion weighting factor, and  $\mathbf{D}$  is the diffusion tensor. The product  $\mathbf{g}_i \mathbf{D} \mathbf{g}_i^T$  represents the diffusivity in the direction  $\mathbf{g}_i$ . For the interpolation of DW images, usual scalar image interpolations can be directly applied to  $S_i$ .

Interpolation essentially consists in finding a continuous image  $s(x, y)$  from its discrete samples  $s(k, l)$  with  $s, x, y \in \mathbb{R}$  and  $k, l \in \mathbb{N}^0$ . It can be described formally as the convolution of the discrete image samples with the continuous impulse response  $h(x, y)$  of a reconstruction filter. The crucial element of any interpolation technique is the interpolation kernel, which distinguishes different interpolation techniques and determines their performance. The conventional interpolation kernels are isotropic and space-invariant (kernel profiles are invariable with respect to orientation and position) and therefore exhibit the drawback of disregarding local image features, such as boundaries [13]. Based on this remark, the anisotropic interpolation method with the sigmoid kernel was proposed for DTI data [10]. This method is space-variant and can suppress noise without compromising the sharpness of boundaries.

The sigmoid kernel function in 1-D case is defined by

$$h(x) = \begin{cases} \frac{1}{1 + \exp(a(x - h))}, & 0 < x < 1 \\ 0, & \text{elsewhere} \end{cases} \quad (1)$$

where  $a$  regulates the sharpness of  $h(x)$  (a larger  $a$  gives a sharper  $h(x)$ ), and  $h$  controls the position of the maximum change in magnitude.

The 2-D or 3-D sigmoid kernel is calculated as the product of symmetrical 1-D sigmoid kernels to reduce computational complexity:

$$h(x, y) = h(x) \times h(y). \quad (2)$$

For 2-D or 3-D scalar images, the sharpness of the sigmoid kernel function is adapted to the local image intensity gradient in each spatial direction [10] using  $a_i = a_{\min} + (a_{\max} - a_{\min}) \times |\nabla I_i / \nabla I_{\max}|$  with  $|\nabla I_{\max}|$  being the maximum intensity gradient of the image, and  $a_{\max}$  and  $a_{\min}$  delimiting the linear mapping between  $a$  and  $|\nabla I|$  so that  $a$  will fall into a proper range. In this study,  $h$  is set to 0.5.

Take a 2-D image for example. Let  $R(x, y)$  represent the original image,  $R(xx, yy)$  the interpolated image, and  $K$  the interpolation factor. The algorithm of anisotropic DW interpolation can be described as follows.

```

For x=1:N_rows
  For y=1:N_cols
    xx = x * K - (K - 1)
    yy = y * K - (K - 1)
    For i=1:K //Note: K is the interpolating factor
      {
        a_x = |\nabla I_x / \nabla I_{\max}| * |R(x, y+1) - R(x, y)| / I_{\max}
        a_{x+1} = |\nabla I_x / \nabla I_{\max}| * |R(x+1, y+1) - R(x+1, y)| / I_{\max}
        R(xx, yy + i) = R(x, y) * \frac{1}{1 + \exp(a_x * (i/K - \eta))}
                       + R(x, y+1) * (1 - \frac{1}{1 + \exp(a_x * (i/K - \eta))})
        R(xx + K, yy + i) = R(x+1, y) * \frac{1}{1 + \exp(a_{x+1} * (i/K - \eta))}
                       + R(x+1, y+1) * (1 - \frac{1}{1 + \exp(a_{x+1} * (i/K - \eta))})
      }
    Endfor
    For j=1:K
      a_y = \frac{|\nabla I_y / \nabla I_{\max}| * |R(xx, yy + j - 1) - R(xx + K, yy + j - 1)|}{I_{\max}}
      For ii=1:K
        R(xx + ii, yy + j - 1) =
          R(xx, yy + j - 1) * \frac{1}{1 + \exp(a_y * (ii/K - \eta))}
          + R(xx + K, yy + j - 1) * (1 - \frac{1}{1 + \exp(a_y * (ii/K - \eta))})
      Endfor
    Endfor
  Endfor
Endfor
    
```

Using the sigmoid kernel function, anisotropic interpolation at DW level preserves a sharp edge of original DW image and subsequently a sharp edge of corresponding tensor fields.

## B. Diffusion Tensor Field Interpolation

For the interpolation of diffusion tensors, anisotropic interpolation [10], [14], PDE interpolation [16], spline interpolation [17], Cholesky interpolation [18], Riemannian interpolation [20], [19], log-Euclidean interpolation [15] and Geodesic-loxodrome interpolation [21], [22] were proposed. In this study, we focus on the log-Euclidean interpolation [15], which reduces the computational complexity of Riemannian calculation while preserving the positive-definite property of diffusion tensors and avoiding swelling effect, and the quaternion interpolation [23], which preserves the advantage of the log-Euclidean method and additionally avoids the FA/MD decrease.

1) *Log-Euclidean Interpolation*: To avoid the swelling effect in processing diffusion tensors, the authors of [15] proposed to work on the nature logarithm of the tensor matrix. The log-Euclidean interpolation of diffusion tensors consists of first performing the logarithm of the original tensors, then interpolating between the logarithmical matrices, and finally reconstructing the interpolated tensors using matrix exponential. The procedure of log-Euclidean interpolation can be described as follows:

$$\begin{cases} \mathbf{L}_0 = \log(\mathbf{D}_0), \quad \mathbf{L}_1 = \log(\mathbf{D}_1) \\ \mathbf{L}(t) = (1-t)\log(\mathbf{L}_0) + t\log(\mathbf{L}_1) \\ \mathbf{D}(t) = \exp(\mathbf{L}(t)). \end{cases} \quad (3)$$

Note that the log-Euclidean method interpolates by essence each element of the transformed matrix (tensor matrix in algorithm).

2) *Tensor Field Interpolation Using Quaternion*: As mentioned before, log-Euclidean interpolation avoids the swelling effect and preserves the positive-definite property of a diffusion tensor. However, it interpolates matrix components independently and ignores the relationship between matrix elements. In order to take into account the relationship between tensor components, a new interpolation method using quaternion was proposed, which decomposes a diffusion tensor into its two features: tensor shape and size, and tensor orientation, with its three eigenvalues representing the tensor shape and size and a unit quaternion representing the tensor orientation. The details about the implementation steps of quaternion tensor interpolation can be found in [23].

Instead of interpolating matrix elements, the quaternion interpolation interpolates the tensor features (eigenvalues and orientation), while the additional work is to obtain the unique quaternion from  $2^3$  possibilities of rotational matrices for a diffusion tensor. Since the determinant of a rotation matrix should equal  $+1$ , not all the eigenvector matrices constructed from  $\mathbf{v}_i = [v_{i1} \ v_{i2} \ v_{i3}]^T$  and  $-\mathbf{v}_i = [-v_{i1} \ -v_{i2} \ -v_{i3}]^T$  are rotation matrices. Consequently, there are four possible eigenvector matrices for choosing a rotation matrix. However, the quaternions  $q$  and  $-q$  representing the same rotation, these four eigenvector matrices correspond to eight quaternions. To obtain the unique quaternion for Step 2 above, we first consider all the pairs of quaternions for the two current tensors to be interpolated by computing their inner product which is calculated in the same way as that for two vectors. The biggest inner product may



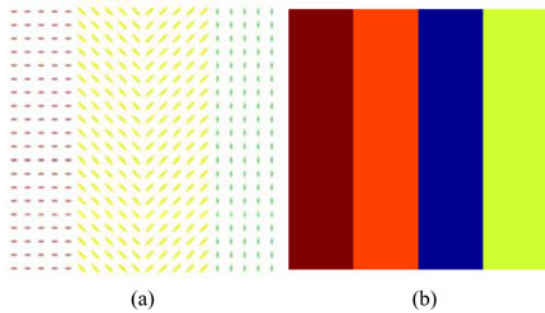


Fig. 1. Synthetic tensor field and the corresponding DW images. (a) Original tensor field. (b) Corresponding DW image at the gradient direction of  $[0 \ 0.5 \ 1]^T$ .

correspond to more than one pair of quaternions. Then, by making use of neighborhood information, the final pair of quaternions corresponding to the current tensors is determined by choosing the one that gives the biggest inner product between each of the two current tensors and its neighboring tensors.

### III. EXPERIMENTS AND RESULTS

To evaluate the performance of different interpolation strategies for the improvement of spatial resolution of DTI and their impact on the analysis of clinical parameters, both synthetic tensor data and real DTI data are used, and the interpolation results are both qualitatively and quantitatively assessed. Note that all the interpolations performed in the present experiments are 3-D. But, they are visualized in 2-D for easier visual assessment.

#### A. Synthetic Data

A diffusion tensor  $\mathbf{D}$  is a  $3 \times 3$  symmetric, positive-definite matrix which can be decomposed as follows:

$$\mathbf{D} = \begin{pmatrix} D_{11} & D_{12} & D_{13} \\ D_{21} & D_{22} & D_{23} \\ D_{31} & D_{32} & D_{33} \end{pmatrix} = \mathbf{R} \begin{pmatrix} \lambda_1 & 0 & 0 \\ 0 & \lambda_2 & 0 \\ 0 & 0 & \lambda_3 \end{pmatrix} \mathbf{R}^T \quad (4)$$

where  $\lambda_1, \lambda_2, \lambda_3$  are eigenvalues of  $\mathbf{D}$  and  $\mathbf{R}$  is the eigenvector matrix.

We generated a  $20 \times 20$  synthetic tensor field containing four different homogeneous regions separated by discontinuities of different orientations of tensors [see Fig. 1(a)]. Tensors in the four regions have the same eigenvalues  $[5 \ 1 \ 1]$ , but different eigenvector matrices:

$$\begin{bmatrix} 1 & 0 & 0 \\ 0 & 1 & 0 \\ 0 & 0 & 1 \end{bmatrix}, \begin{bmatrix} 1 & 1 & 0 \\ 1 & -1 & 0 \\ 0 & 0 & 1 \end{bmatrix}, \begin{bmatrix} 1 & -1 & 0 \\ 1 & 1 & 0 \\ 0 & 0 & 1 \end{bmatrix} \text{ and } \begin{bmatrix} 0 & 1 & 0 \\ 1 & 0 & 0 \\ 0 & 0 & 1 \end{bmatrix}.$$

We used the Stejskal–Tanner diffusion equations to compute the DW images [see Fig. 1(b)] from this synthetic tensor field. The associated  $S_0$  image was chosen to be constant and we considered the truncated octahedron encoding scheme (12 directions) to simulate the gradient directions.

#### B. Real DTI Data

The real DTI datasets were acquired in clinical conditions. They concern the cardiac DW images and T2 images, which were acquired from eight *ex vivo* human hearts on Siemens 1.5 T Magnetom Sonata with the following settings: TE = 98 ms, TR = 8600 ms, FOV =  $256 \times 256 \text{ mm}^2$ , slice thickness = 2 mm, slice spacing = 2 mm, slice duration = 142.5 ms, number of slices = 52, number of  $b = 0$  slice images = 52,  $128 \times 128$  pixels in each slice, diffusion sensitivity  $b = 1000 \text{ s/mm}^2$ , and gradient directions = 30 or 12 or 6. The acquisition time for a 3-D dataset with 30 directions and 1 average is 4.6 min. Each heart was located in a plastic container and fixed by hydrophilic gel to maintain a diastolic shape. This setup has a low dielectric effect and also eliminates unwanted susceptibility artifacts near the boundaries of the heart.

#### C. Performance Evaluation

The comparison of the different interpolation methods was performed in a qualitative and quantitative manner, by means of tensor fields, tensor parameter maps, and fiber tractography.

*Tensor fields:* In the case of tensor fields, we compare the variation of tensor shape and tensor orientation.

*Tensor parameter maps:* When considering tensor parameter maps, we compare the MD, FA, and determinant maps computed from the interpolated tensor fields. MD indicates the mean diffusivity of water molecules, which reflects the redistribution of intracellular and extracellular space volumes. FA is defined as

$$\text{FA} = \left\{ \frac{3[(\lambda_1 - \bar{\lambda})^2 + (\lambda_2 - \bar{\lambda})^2 + (\lambda_3 - \bar{\lambda})^2]}{2(\lambda_1^2 + \lambda_2^2 + \lambda_3^2)} \right\}^{1/2} \quad (5)$$

where  $\bar{\lambda}$  is the mean of the three eigenvalues of the diffusion tensor  $\lambda_1, \lambda_2, \lambda_3$ , which represents in fact the MD. FA ranges from 0 for isotropic diffusion to 1 for completely anisotropic diffusion. More quantitative criteria have also been used that concern the tensor determinant and the standard deviation (STD) of FA or MD, which is calculated as

$$\text{STD}(X) = \sqrt{\frac{1}{M \times N} \sum_{i=1}^M \sum_{j=1}^N (X(i, j) - \bar{X})^2} \quad (6)$$

where  $X$  indicates the FA or MD value of the original or interpolated diffusion tensors, and  $\bar{X}$  the mean FA or MD value.

Tensor determinant is proportional to the volume of ellipsoid and is calculated as

$$\det(D) = \lambda_1 \lambda_2 \lambda_3. \quad (7)$$

Determinant maps were used to check whether the interpolation methods introduce swelling effect which should be avoided by DTI processing [15], [19].

*Fiber tractography:* To illustrate the influence of different interpolations on fiber tractography, quantitative comparisons in terms of the number and length of fibers are given.

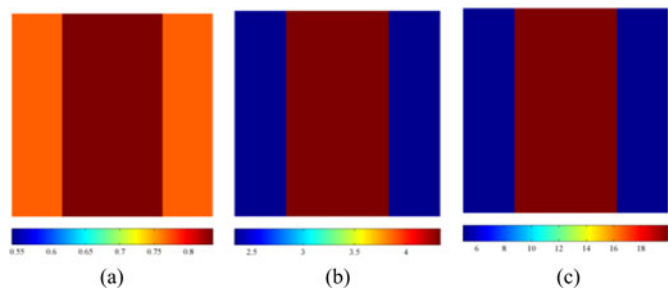


Fig. 2. Original parameter maps from the tensor field. (a) FA map. (b) MD map (unit:  $10^{-4}$ ). (c) Determinant.

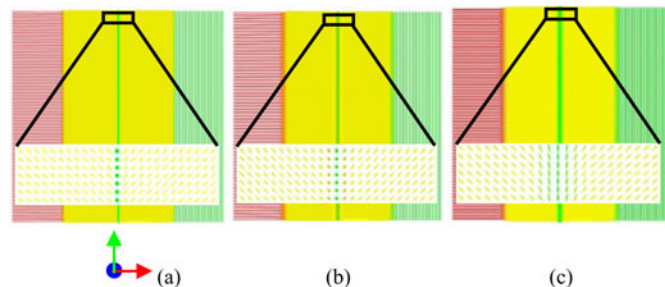


Fig. 3. Interpolated tensor fields obtained after performing interpolation (a) at the level of DW image, (b) at the level of tensor field with the log-Euclidean method, and (c) at the level of tensor field with quaternions.

#### D. Results

1) *Synthetic Data*: The anisotropic interpolation was applied to synthetic DW images and log-Euclidean interpolation to the synthetic tensor fields [see Fig. 1(a)]. The original size of  $20 \times 20$  was interpolated to the size of  $153 \times 153$ . To compare the interpolation methods at different levels, tensor field and parameter maps from tensor fields were calculated.

Fig. 1 shows the generated synthetic tensor field and the corresponding DW images in 12 diffusion gradient directions, while Fig. 2 indicates the parameter maps calculated from the tensor field. It is to underline that the three original parameter maps present three homogeneous regions.

Fig. 3 shows the interpolated tensor fields obtained using anisotropic interpolations at the level of DW images and log-Euclidean interpolation at the level of tensor fields. The color of the ellipsoid is determined by the primary eigenvector direction of the tensor. The tensor fields being too dense, we zoomed the black-boxed regions. Compared with the original tensor field, it is observed that tensors with different orientations or shapes (vertical green line and/or its neighbors) have been introduced by both DW interpolation and log-Euclidean tensor field interpolation although the original tensors all have the same shape, whereas with the log-Euclidean interpolation at the level of tensor fields, sphere-like tensors were introduced not only on the vertical green line but also in the two sides of the latter. Note that on this extra green vertical line, the volume of tensors produced by the anisotropic interpolation at the level of DW images is bigger than that interpolated by the log-Euclidean interpolation at the level of tensor fields. On the other hand, for the same DW interpolation, the interpolated tensors on and around the vertical

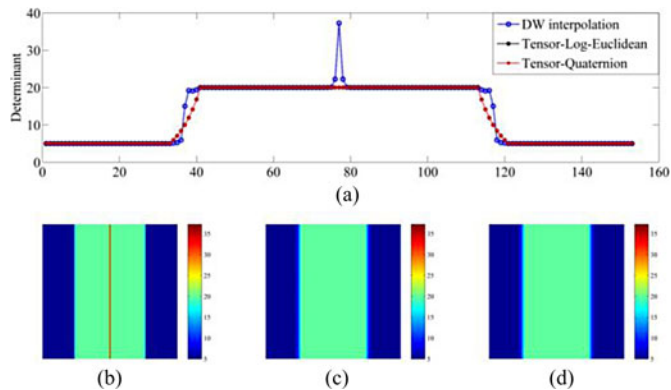


Fig. 4. Determinant maps from interpolations at the DW image and tensor field levels. (a) Comparison of determinant profiles with different methods. (b) Determinant map with anisotropic interpolation at the level of DW images. (c) Determinant map with log-Euclidean interpolation at the level of tensor fields. (d) Determinant map with quaternion interpolation at the level of tensor fields.

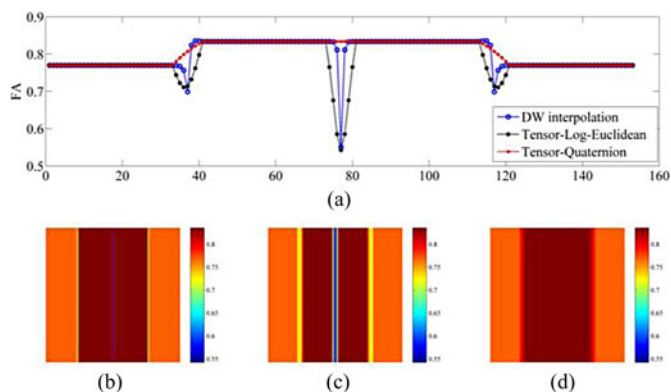


Fig. 5. FA maps interpolations at the DW image and tensor field levels. (a) Comparison of FA profiles with different methods. (b) FA map with anisotropic interpolation at the level of DW images. (c) FA map with log-Euclidean interpolation at the level of tensor fields. (d) FA map with quaternion interpolation at the level of tensor fields.

green line have bigger volume than the rest of the tensors. This swelling effect can also be clearly observed on the determinant map in Fig. 4, by the presence of the vertical red line that divides the green homogeneous region into two parts. More quantitatively, between two original tensors having a determinant of 20, the DW interpolation generates two interpolated tensors having a determinant of 22 and a third interpolated tensor having a determinant of 37. In contrast, log-Euclidean and quaternion interpolations at the level of tensor fields preserved this homogeneous region present in the original determinant map (the tensor determinant was kept 20). Also note that on the borders between the blue and green regions, anisotropic interpolation at the level of DW images produced sharper edges than log-Euclidean and quaternion interpolations at the level of tensor fields.

In Fig. 5 are plotted the FA maps and FA profiles obtained using anisotropic interpolations at the level of DW images and log-Euclidean and quaternion interpolations at the level of tensor fields. As observed, both DW image interpolation and log-Euclidean tensor field interpolation led to the FA collapse between two original homogeneous regions by the presence of the

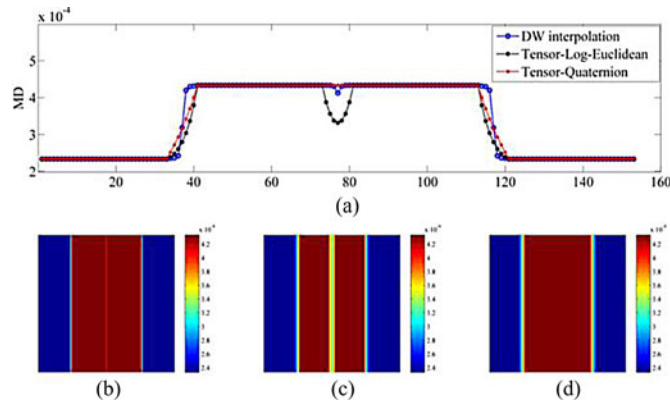


Fig. 6. MD maps from interpolations at the DW image and tensor field levels. (a) Comparison of MD profiles with different methods. (b) MD map with anisotropic interpolation at the level of DW images. (c) MD map with log-Euclidean interpolation at the level of tensor fields. (d) MD map with quaternion interpolation at the level of tensor field.

extra vertical lines (caused by the abrupt decrease of FA values) with sharp different colors. As in the case of determinant maps, the DW image interpolation produced much sharper edges than the log-Euclidean tensor field interpolation. In contrast, the quaternion method at the tensor field level preserved FA values during interpolation and therefore preserved the homogeneous regions present in the original FA map.

Similar phenomenon is observed in the MD maps and profiles (see Fig. 6), in which the decrease of MD values with DW interpolation and log-Euclidean tensor field interpolation occurred between the two central regions where the tensors have the same shape but different orientations. Note that the decreasing effect introduced by log-Euclidean interpolation at the level of tensor fields is much greater than that at the level of DW images.

2) *Real Data*: The interpolation methods at the two levels were applied to the datasets acquired in clinical conditions. We choose to illustrate the tenth slice of a human cardiac DTI volume since it is near the heart base where both right and left ventricles are visible. The initial slices of  $128 \times 128$  were interpolated to a size of  $512 \times 512$ .

Fig. 7 shows the FA map calculated from the original tensor field of the tenth slice and the FA maps from the interpolated tensor fields obtained using anisotropic interpolation at the level of DW images and log-Euclidean and quaternion interpolations at the level of tensor fields. The black pixels in the original FA map indicate where the eigenvalues are negative because of noise, and the subsequent FA values calculated are greater than 1. We observe that, with anisotropic interpolation at the level of DW images, noisy areas are enlarged; namely, unreasonable pixels ( $FA > 1$ ) are interpolated. By contrast, with log-Euclidean and quaternion interpolations at the level of tensor fields, noisy pixels where FA values are greater than 1 have disappeared. To better compare the three different methods, we plot in Fig. 8 the profiles (corresponding to the red line in the original FA map in Fig. 7) of the FA maps. In the profile with anisotropic interpolation at the DW level, there is a FA peak greater than 1, which is incoherent. In the zoomed profiles, the circled points represent the original data points. With both the anisotropic interpolation at the level of DW images and the log-Euclidean

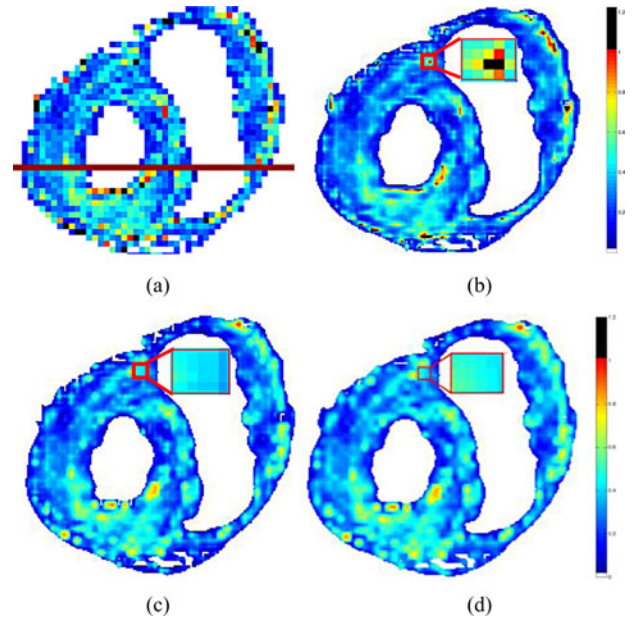


Fig. 7. FA maps calculated from the original tensor fields as well as the interpolated tensor fields using different interpolations, for real human cardiac DTI data. (a) FA map of the original DTI slice. (b) FA map after anisotropic interpolation at the DW image level. (c) FA map from log-Euclidean interpolation at the level of tensor fields. (d) FA maps from quaternion interpolation at the level of tensor fields.

interpolation at the level of tensor fields, there is FA decreasing effect (the interpolated FA values are smaller than the two original FA values). In addition, with the DW image interpolation, the FA decreasing effect is more severe than with the tensor field interpolation and the interpolated FA values vary in an irregular manner. However, the quaternion interpolation at the level of tensor fields interpolated FA values without decreasing effect or sharp peak values of FA.

Concerning the MD values (see Fig. 9), both anisotropic interpolation at the level of DW images and the two interpolation methods at the level of tensor fields introduced MD value jumped at the borders, while in other regions, the anisotropic interpolation at DW image level and the log-Euclidean interpolation at the tensor field level may induce MD decreasing effect (the interpolated MD values are smaller than the two original MD values), whereas the quaternion interpolation at the tensor field level avoids the decrease in the interpolated MD values.

In order to further get insights into the influence of interpolation methods on FA and MD values, we divide the left myocardium into six sectors, and then statistical analysis of FA and MD values is performed in terms of mean value and STD in three situations: 1) on different sectors of the same slice; 2) on the same sector but for different slices of the same heart; and 3) on the same sector of the same slice of different hearts. Fig. 10(a) shows the spatial distribution of the six sectors in a slice, and Fig. 10(b) [or 10(c)] the variation of mean FA (or MD) values as a function of sector number in the tenth slice of a human heart. It is observed that the mean FA values obtained using both anisotropic interpolation at the DW image level and log-Euclidean interpolation at the tensor field level decrease,



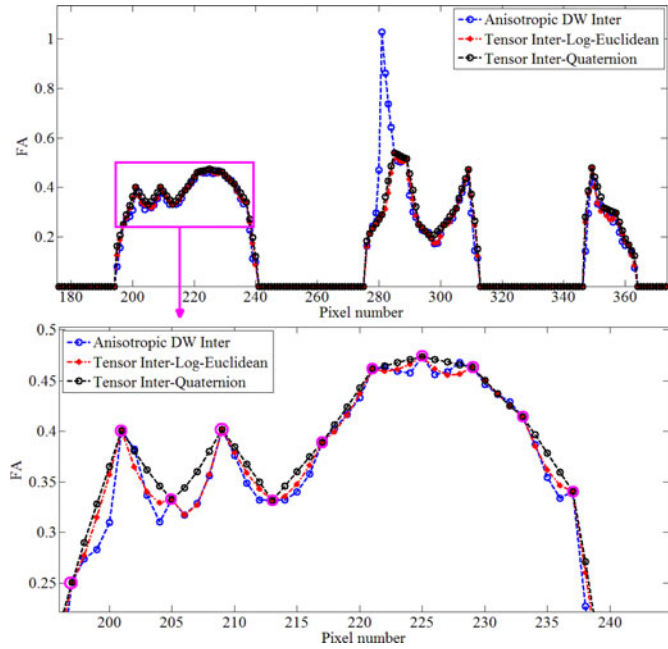


Fig. 8. FA profiles corresponding to the dark red line in Fig. 7. The bottom plot corresponds to the zoomed version of the boxed part in the top plot to better visualize FA collapse effects caused by interpolation. The three curves in the plots correspond to anisotropic interpolation at DW image level (blue line) and log-Euclidean interpolation at the tensor field level (red line), and quaternion interpolation at the tensor field level (black line), respectively. The pink circled points represent the original data points.

compared to the mean FA values before interpolation, while the mean FA values with log-Euclidean tensor field interpolation are closer to those of the original tensor field. In contrast, the mean FA values obtained using the quaternion interpolation is bigger than those before interpolation. Concerning the mean MD curves, we can see that the mean MD values with anisotropic DW interpolation are higher than the original ones, whereas the mean MD values with log-Euclidean and the quaternion tensor field interpolation coincide most time with the original MD curve with sometimes alternating greater and smaller value with respect to the original mean MD values. These variations of FA and MD are also observed from the FA and MD values calculated in the same sector but in different slices (see Fig. 11), and from the FA and MD values calculated in the same sector of the same slice for different human hearts (see Fig. 12).

In terms of STD of FA or MD, the obtained results showed that the STDs of FA values before and after interpolation (at the DW or tensor field level) are not very different, and that they oscillate around 0.13. This is true for the three situations mentioned previously. With regard to STDs of MD values, they are about  $2 \times 10^{-4}$ . Note, however, that the STDs of FA values obtained after interpolation (no matter whatever the interpolation level is) are smaller than those before interpolation. In contrast, the STDs of MD values exhibit somewhat irregular behavior following the used interpolation. Using the log-Euclidean tensor field interpolation, the STDs of resulting MD values become

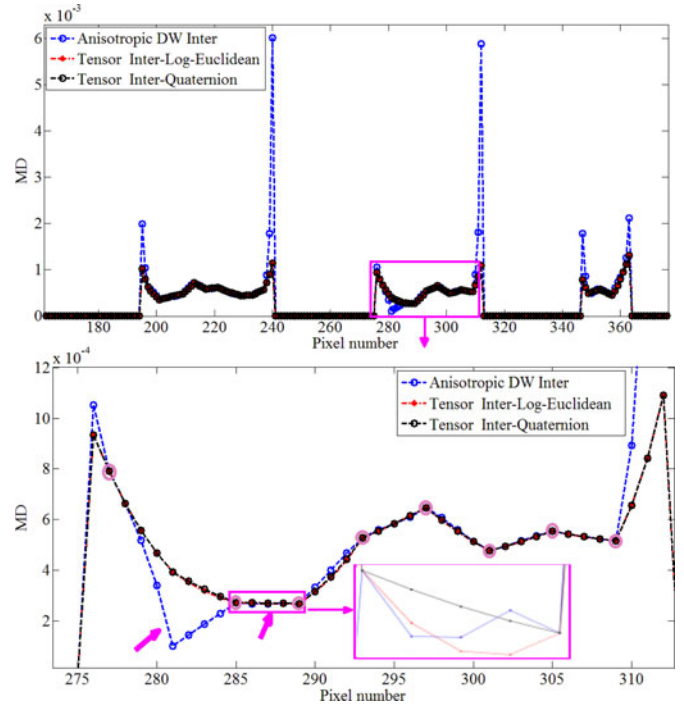


Fig. 9. MD profiles corresponding to the dark red line in Fig. 7. The zoomed version of the boxed part in the top plot is given in the bottom plot. The pink arrows, one of which indicates a zoomed part to better visualize the slight MD decreasing effects, indicate where there exist MD decreasing effects caused by both anisotropic interpolation at the DW image level (blue line) or log-Euclidean interpolation at the level of tensor fields (red line), but not by quaternion interpolation at the tensor field level (black line).

slightly smaller than those calculated from the original tensor field, whereas, using anisotropic DW level interpolation, the STDs of the obtained MD values become greater or smaller than those of original MD values. The increasing of the STDs of MD values after DW interpolation is due to the presence of boundaries in the images, as can be observed in Fig. 9.

To describe more quantitatively the null or negative eigenvalues induced by the DW image interpolation, we define the number of null or negative eigenvalues of tensors. Fig. 13 shows the number of tensors presenting null or negative eigenvalues in the original or interpolated tensor fields with different interpolation methods. Null or negative eigenvalues appear when there exist noises or artifacts in the original data. After interpolation, it is observed that neither of the three interpolation methods introduced null or negative eigenvalues when there are no null or negative eigenvalues in the original data. However, when null or negative eigenvalues are present in the original data, DW anisotropic interpolation produced more null or negative eigenvalues, from one to three times of the original data, whereas log-Euclidean interpolation or quaternion interpolation did not introduce any null or negative eigenvalues.

Fiber tractography is a technique allowing us to visualize the fibers of the tissues under investigation. To evaluate the influence of the interpolation methods on the fiber tractography, we used in this study the streamline fiber tractography method (fourth-order Runge-Kutta integration) [26]. The original tensor fields of  $128 \times 128 \times 52$  were interpolated to  $512 \times 512 \times 52$ . During

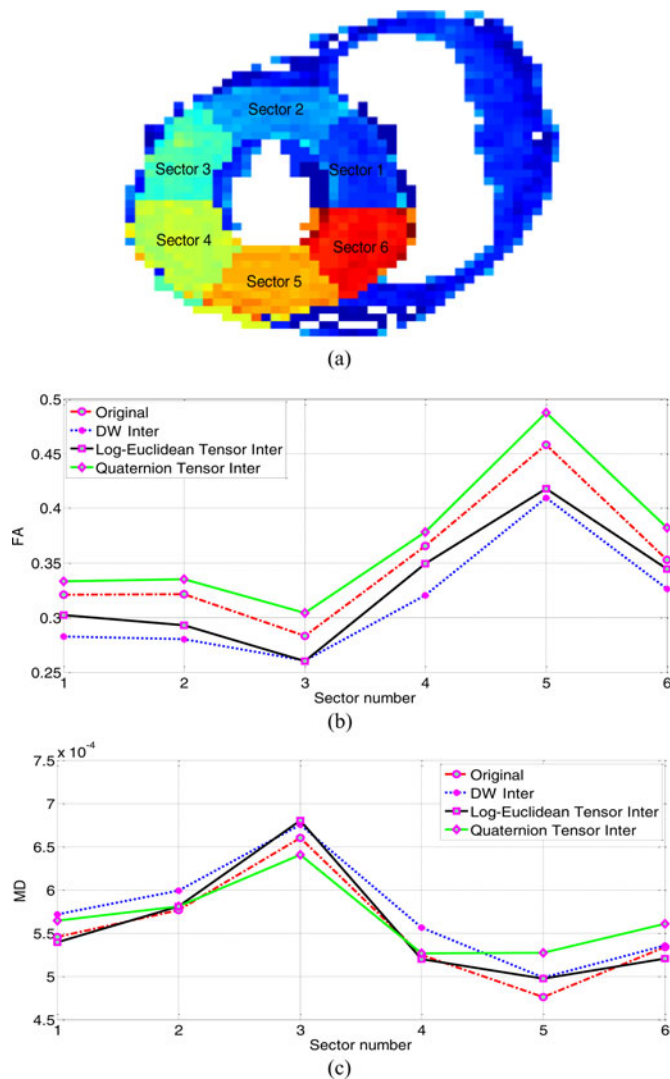


Fig. 10. Comparison of FA and MD mean values in six uniformly distributed sectors in the same slice (tenth slice) of a human heart. (a) Spatial distribution of the six sectors distributed in the left ventricle. (b) FA and (c) MD mean curves from the original tensor field (red line) and the tensor fields interpolated using DW interpolation (blue line), log-Euclidean tensor field interpolation (black line), and quaternion tensor field interpolation (green line).

fiber tracking using the streamline method, the minimum fiber length was limited to 20 mm, and the FA threshold was set at 0.1. The 3-D fiber tractography of the left heart of a healthy human heart with different methods is displayed in Fig. 14, in which the visualization results are shown in top and lateral views. All three interpolation methods led to the similar spiral fiber architecture of the myocardium. The pink arrows indicate where the fibers produced by anisotropic interpolation at the level of DW images are denser than those obtained with log-Euclidean interpolation at the level of tensor fields but are less dense than the quaternion interpolation at the level of tensor fields, while the black arrows show where the two interpolation methods at the level of tensor fields produced denser fibers than the one at the level of DW images. More quantitatively, comparison between the two level interpolations in terms of the number of fibers, mean length, and STD of fibers is demonstrated in Fig. 15. We observe that,

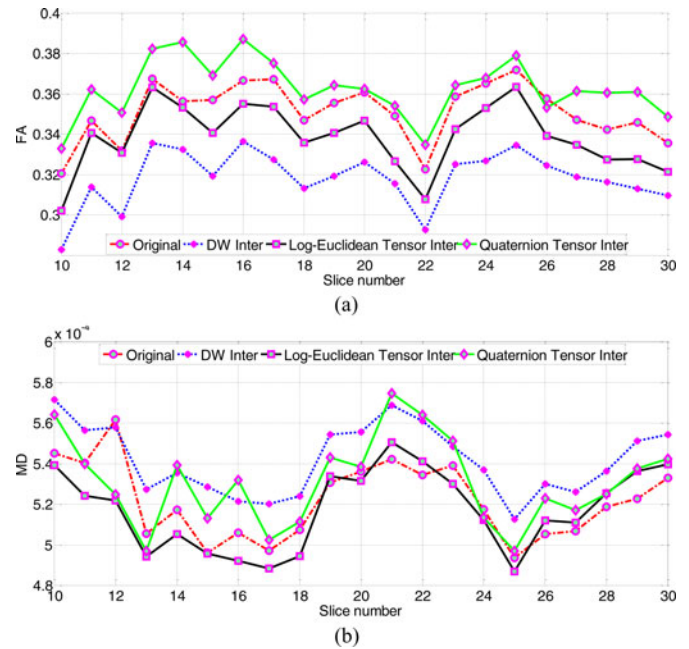


Fig. 11. Mean FA (a) and mean MD (b) curves of the original tensor field (red line) and the tensor fields interpolated with DW interpolation (blue line), log-Euclidean tensor field interpolation (black line), and quaternion tensor field interpolation (green line) in Sector 1 of Fig. 10(a) for different slices of the same heart.

in general, log-Euclidean and the quaternion interpolations at the level of tensor fields produced more and longer fibers than anisotropic interpolation at the level of DW images, but with insignificant difference in mean fiber length (the largest length difference between the three methods is 2 or 3 voxels).

#### IV. DISCUSSION

As mentioned for the interpolated tensor fields, anisotropic interpolation at the level of DW images introduced less sphere-like tensors than log-Euclidean interpolation at the level of tensor fields. This is due to the fact that the DW image interpolation is an anisotropic interpolation technique, which has the characteristic of keeping the sharpness of image edges. As a result, anisotropic interpolation at the level of DW images produces tensor fields, FA and MD maps with sharp edges, which means that the edges are closer to the original ones with the DW level interpolation than with log-Euclidean tensor level interpolation. However, DW image interpolation could introduce swelling effect and artifacts in the subsequent determinant map (extra vertical line in the determinant map). Nevertheless, compared to log-Euclidean tensor interpolation, using anisotropic DW interpolation introduces less serious artifacts in FA and MD maps. In contrast, the quaternion interpolation at the level of tensor fields preserves tensor shape and consequently preserves the homogeneous regions present in the original tensor field, determinant, FA and MD maps.

In the case of noisy DTI data such as real cardiac DTI data, anisotropic interpolation at the level of DW images may amplify the noise, and cannot guarantee the positive-definiteness properties of tensors. This explains the presence of enlarged black



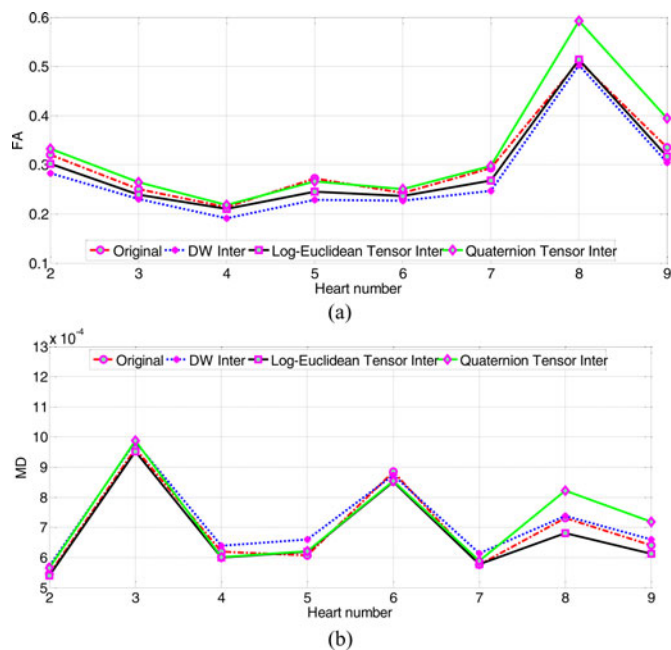


Fig. 12. Mean FA (a) and mean MD (b) curves of the original tensor field (red line) and the tensor fields interpolated with DW image interpolation (blue line), log-Euclidean tensor field interpolation (black line), and quaternion tensor field interpolation (green line) in the same sector (Sector 1) of the same slice (tenth slice) for different hearts.

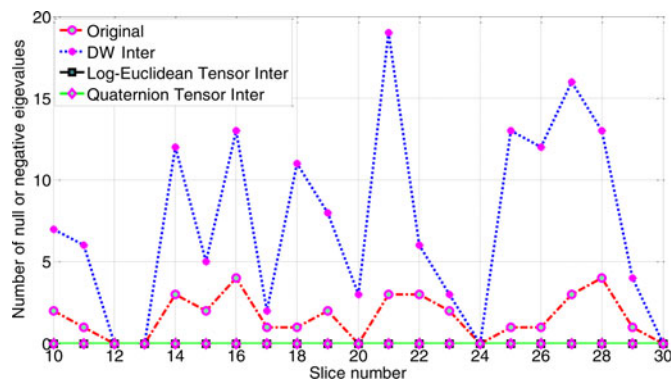


Fig. 13. Number of null or negative eigenvalues of the original (red line) and interpolated tensor fields using DW interpolation (blue line), log-Euclidean tensor field interpolation (black line), and quaternion tensor field interpolation (green line) in Sector 1 of Fig. 10(a) for different slices of the same heart.

areas presenting unreasonable FA values (see Fig. 7). In contrast, log-Euclidean and quaternion tensor interpolations do not produce tensors with unreasonable FA values (or unreasonable eigenvalues) since the positive-definite property of tensors is ensured when taking the logarithm of tensors. Meantime, small areas formed of a few pixels having different but close values are preserved after log-Euclidean and quaternion interpolations, demonstrating that they are loyal to the underlying data (isolated structures or not) while removing noisy points. This is, however, difficult for DW image level interpolation since when performed on DW images, interpolation does not guarantee the positivity of the interpolated eigenvalues due to the nonlinear process from DW images to a tensor. Similarly, for FA and MD values, since after nonlinear equations from DW images to dif-

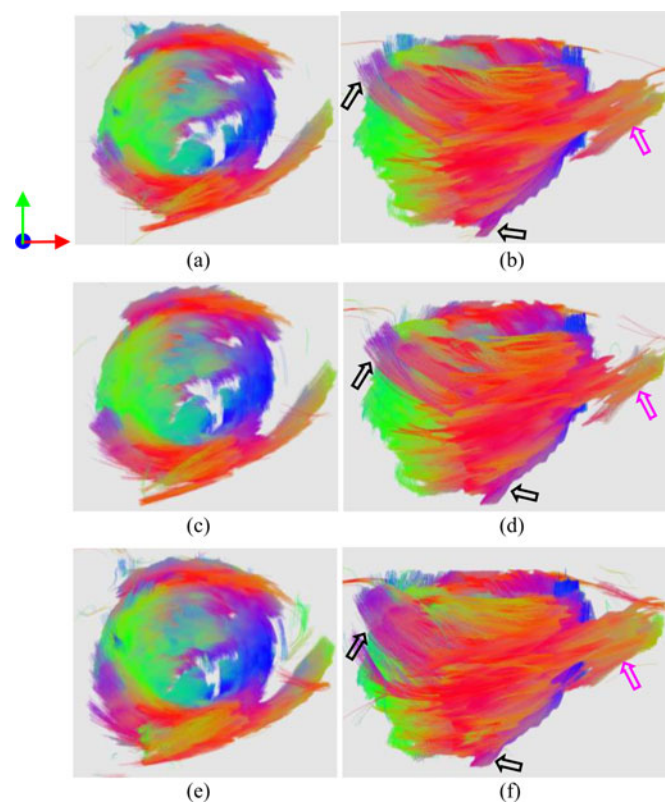


Fig. 14. Fiber tractography from the tensor fields interpolated with the different methods, for real human cardiac DTI data. The first and second columns, respectively, indicate lateral views and top view of left myocardial fiber architecture. (a) and (b) Interpolation at the DW image level. (c) and (d) Interpolation at the level of tensor fields using log-Euclidean method. (e) and (f) Interpolation at the level of tensor fields using quaternion method. The color designates the direction of the primary eigenvector (red: left/right; blue: anterior/posterior; green: bottom/top).

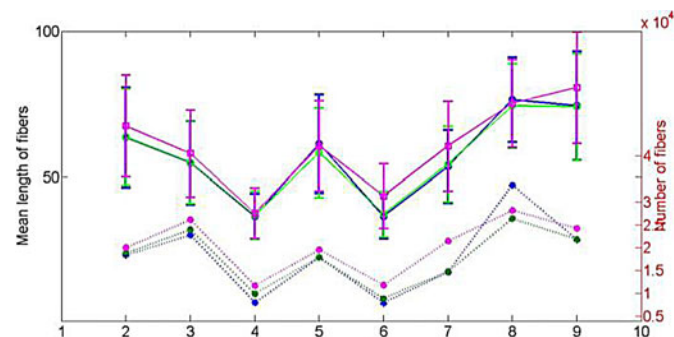


Fig. 15. Parameters of fibers passing through a given slice derived from the fiber tractography of the whole heart in eight human datasets. The three upper solid lines indicate the mean length and STD of fibers with DW image interpolation (in blue), log-Euclidean tensor interpolation (in green), and quaternion tensor interpolation (in pink), while the three lower dotted lines indicate the number of fibers with DW image interpolation (in blue), log-Euclidean tensor interpolation (in green), and quaternion tensor interpolation (in pink).

fusion tensors, the interpolated tensor properties such as FA and MD are unpredictable, which explains the irregular values of FA and MD profiles (see Figs. 7 and 8). In contrast, even though log-Euclidean interpolation at the level of tensor fields also introduced FA and MD decreasing effects, the interpolated tensor values are readily deduced from its interpolation formula, from

which tensor properties can be consequently deduced. Based on these deductions, it is possible to propose new methods to avoid the drawbacks of tensor field interpolation. For example, to avoid the decreasing effect of FA/MD values, quaternion interpolation at the tensor field level is proposed, which can be observed from the FA profiles in Figs 10, 11, and 12. In addition, it should be noted that the number of noise points increases when using DW image interpolation (see Fig. 13); that is, DW interpolation introduces artifacts which is not proportional to the interpolation factor.

The FA collapse with DW image interpolation or log-Euclidean interpolation, which is observed in Fig. 8, implies that the interpolated FA values with the two methods are smaller than the smallest value of the original FA values whereas with the quaternion tensor interpolation method, the interpolated value is always greater than the smallest original FA value and smaller than the greatest original FA value. That is an inherent property of the three methods. However, the FA values in Figs. 10–12 show that the mean quaternion FA curve is above the original mean FA curve. This is because the mean of all FA values including interpolated FA values is always greater than the original mean FA value with the quaternion tensor interpolation. In short, the averaged FA value on a region becomes greater than the original mean FA values when using quaternion tensor interpolation while the average FA value becomes smaller than the original mean FA value when using DW image interpolation or log-Euclidean interpolation.

It is well known that the decrease in FA in the brain may be due to diseases or crossing fibers [27], [28], and that the decrease in FA in the heart is caused by infarction [29]. Therefore, the abrupt decrease in FA (at a single point or averaged FA) induced by the DW image interpolation or log-Euclidean tensor interpolation may mislead the interpretation of the clinical results. Likewise, the effect of FA increasing due to region averaging in the case of quaternion interpolation should also be considered when interpreting the actual FA values.

The results of fiber tractography at the level of DW images and tensor fields are globally similar, but with some small differences. The two tensor field interpolations generate more and longer fibers than DW image interpolation, because the latter amplifies the noise and produces more unreasonable FA values. However, in terms of fiber tractography, the difference in mean fiber length between the tensor field and DW image interpolations is very small. This is perhaps due to the fact that the data points having unreasonable FA values are not sufficiently numerous to significantly influence the fiber tractography. Indeed, in view of the fact that the myocytes in the myocardium are 80 to 100  $\mu\text{m}$  in length [30], [31], the difference between the two different level interpolation methods represents a difference of three or four myocytes in length. So, we can say that the difference between tensor field interpolations and DW image interpolation is insignificant in terms of mean fiber length.

Another interesting approach for diffusion tensor interpolation is to use biquaternion [32] by first transforming a diffusion tensor in log-Euclidean space to a biquaternion and then performing the interpolation on the corresponding biquaternion. The biquaternion convert diffusion tensors from a manifold

space to a vector space, which gives the possibility to preserve the properties of original tensors when performing calculations in a vector space.

## V. CONCLUSION

We have compared different level interpolation strategies for DTI data and their impacts on clinical parameters such as FA and MD. The results on both synthetic and real data showed that interpolation is a feasible and effective way to improve the spatial resolution of DTI data. However, the interpolation at the level of DW gray-level images produces swelling effect which can be avoided by the interpolation at the level of tensor fields. Moreover, the interpolation of tensor fields generates more and longer fibers than the interpolation of DW gray-level images. On the other hand, both the anisotropic DW gray-level image interpolation and log-Euclidean tensor field interpolation introduce FA and MD decrease. Therefore, in clinical analysis, the results involving the use of DW image interpolation or log-Euclidean tensor interpolation should be interpreted with precaution since the abrupt decrease of FA values caused by these methods may lead to the interpretation of the presence of diseases or fiber crossing, whereas the quaternion tensor interpolation can allow avoiding these misleading since it does not introduce decrease in FA and MD values. More generally, with tensor interpolation, we can predict the attributes such as FA and MD of the interpolated tensors and consequently preserve these attributes during interpolation, which is difficult with the interpolation at the level of DW gray-level images due to the nonlinear transformation from DW image to diffusion tensors. All these findings would then suggest that tensor field interpolation would be more convenient than scalar image interpolation for improving DTI.

## REFERENCES

- [1] P. J. Basser, J. Mattiello, and D. Le Bihan, "MR diffusion tensor spectroscopy and imaging," *Biophys. J.*, vol. 66, no. 1, pp. 259–267, Jan. 1994.
- [2] D. Le Bihan, J. F. Mangin, C. Poupon, C. A. Clark, S. Pappata, N. Molko, and H. Chabriat, "Diffusion tensor imaging: Concepts and applications," *Magn. Reson. Imag.*, vol. 13, no. 4, pp. 534–546, Mar. 2001.
- [3] P. J. Basser and S. Pajevic, "Statistical artifacts in diffusion tensor MRI (DT-MRI) caused by background noise," *Magn. Reson. Med.*, vol. 44, no. 1, pp. 41–50, Jul. 2000.
- [4] F. Yang, Y.-M. Zhu, S. Rapacchi, J.-H. Luo, M. Robini, and P. Croisille, "Interpolation of vector fields from human cardiac DTI," *Phys. Med. Biol.*, vol. 56, no. 5, pp. 1415–1430, Mar. 2011.
- [5] F. Yang, X. Song, S. Rapacchi, L. Fanton, P. Croisille, and Y.-M. Zhu, "Noise-reduced TPS interpolation of primary vector fields for fiber tracking in human cardiac DTI," in *Proc. 5th Int. Conf. Funct. Imag. Model. Heart*, Nice, France, 2009, pp. 78–86.
- [6] F. Yang, Y.-M. Zhu, X. Song, J.-H. Luo, and P. Clarysse, "Interpolation of human cardiac DTI data using polar coordinates," in *Proc. Int. Conf. Signal Process.*, Beijing, China, 2010, pp. 678–681.
- [7] F. Yang, Y.-M. Zhu, X. Song, S. Rapacchi, P. Croisille, and M. Robini, "Interpolation et débruitage du champ de vecteurs 3-D en IRM cardiaque du tenseur de diffusion," presented at the Symposium on Signal Processing and Images, Dijon, France, 2009, p. 45.
- [8] T. M. Lehmann, C. Gonner, and K. Spitzer, "Survey: Interpolation methods in medical image processing," *IEEE Trans. Med. Imag.*, vol. 18, no. 11, pp. 1049–1075, Nov. 1999.
- [9] T. M. Lehmann, C. Gonner, and K. S. Addendum, "B-spline interpolation in medical image processing," *IEEE Trans. Med. Imag.*, vol. 20, no. 7, pp. 660–665, Jul. 2001.

- [10] A. Mishra, Y. G. Lu, J. J. Meng, A. W. Anderson, and Z. H. Ding, "Unified framework for anisotropic interpolation and smoothing of diffusion tensor images," *NeuroImage*, vol. 31, no. 4, pp. 1525–1535, Jul. 2006.
- [11] F. Guichard and F. Malgouyres, "Total variation based interpolation," in *Proc. Eur. Signal Process. Conf.*, Island of Rhodes, Greece, 1998, pp. 1741–1744.
- [12] F. Malgouyres and F. Guichard, "Edge direction preserving image zooming: A mathematical and numerical analysis," *SIAM J. Numer. Anal.*, vol. 39, no. 1, pp. 1–37, 2001.
- [13] A. Belahmidi and F. Guichard, "A partial differential equation approach to image zoom," in *Proc. Int. Conf. Image Process.*, Hong Kong, China, 2004, pp. 649–652.
- [14] C. A. Castaño-Moraga, M. A. Rodríguez-Flórido, L. Álvarez, C.-F. Westin, and J. Ruiz-Alzola, "Anisotropic interpolation of DTI," in *Proc. Int. Conf. Med. Image Comput. Comput.-Assisted Intervention Conf.*, Rennes, France, 2004, pp. 343–350.
- [15] V. Arsigny, P. Fillard, X. Pennec, and N. Ayache, "Log-Euclidean metrics for fast and simple calculus on diffusion tensors," *Magn. Reson. Med.*, vol. 56, no. 2, pp. 411–421, Jun. 2006.
- [16] J. Weickert and M. Welk, "Tensor field interpolation with PDEs," in *Visualization and Processing of Tensor Fields*. Berlin, Germany: Springer, 2006, pp. 315–325.
- [17] A. Barmpoutis, B. C. Vemuri, T. M. Shepherd, and J. R. Forder, "Tensor splines for interpolation and approximation of DT-MRI with applications to segmentation of isolated rat hippocamp," *IEEE Trans. Med. Imag.*, vol. 26, no. 11, pp. 1537–1546, Nov. 2007.
- [18] Z. Wang, B. Vemuri, Y. Chen, and T. Mareci, "A constrained variational principle for direct estimation and smoothing of the diffusion tensor field from complex DWI," *IEEE Trans. Med. Imag.*, vol. 23, no. 8, pp. 930–939, Aug. 2004.
- [19] X. Pennec, P. Fillard, and N. Ayache, "A Riemannian framework for tensor computing," *Int. J. Comput. Vis.*, vol. 66, no. 1, pp. 41–66, Jan. 2006.
- [20] P. G. Batchelor, M. Moakher, D. Atkinson, F. Calamante, and A. Connelly, "A rigorous framework for diffusion tensor calculus," *Magn. Reson. Med.*, vol. 53, no. 1, pp. 221–225, Jan. 2005.
- [21] G. Kindlmann, R. S. J. Estepar, M. Niethammer, S. Haker, and C.-F. Westin, "Geodesic-loxodromes for diffusion tensor interpolation and difference measurement," in *Proc. Int. Conf. Med. Image Comput. Comput.-Assisted Intervention*, Brisbane, Australia, 2007, pp. 1–9.
- [22] G. Kindlmann, D. B. Ennis, R. T. Whitaker, and C.-F. Westin, "Diffusion tensor analysis with invariant gradients and rotation tangents," *IEEE Trans. Med. Imag.*, vol. 26, no. 11, pp. 1483–1499, Nov. 2007.
- [23] F. Yang, Y.-M. Zhu, I. E. Magnin, J.-H. Luo, P. Croisille, and P. B. Kingsley, "Feature-based interpolation of diffusion tensor fields and application to human cardiac DTI," *Med. Image Anal.*, vol. 16, no. 2, pp. 459–481, Feb. 2012.
- [24] F. Yang, Y.-M. Zhu, M. Robini, and P. Croisille, "DT-MRI interpolation: At what level?" in *Proc. Int. Conf. Signal Process.*, 2012, pp. 737–740.
- [25] E. O. Stejskal and J. E. Tanner, "Spin diffusion measurements: Spin echoes in the presence of a time-dependent field gradient," *J. Chem. Phys.*, vol. 42, no. 1, pp. 288–292, Dec. 1965.
- [26] P. J. Basser, S. Pajevic, C. Pierpaoli, J. Duda, and A. Aldroubi, "In vivo fiber tractography using DT-MRI data," *Magn. Reson. Med.*, vol. 44, no. 4, pp. 625–632, Oct. 2000.
- [27] A. Virda, A. Barnett, and C. Pierpaoli, "Visualizing and characterizing white matter fiber structure and architecture in the human pyramidal tract using diffusion tensor MRI," *Magn. Reson. Imag.*, vol. 17, no. 8, pp. 1121–1133, Oct. 1999.
- [28] C. Pierpaoli and P. J. Basser, "Toward a quantitative assessment of diffusion anisotropy," *Magn. Reson. Med.*, vol. 36, no. 6, pp. 893–906, Dec. 1996.
- [29] M. Wu, W. I. Tseng, M. M. Su, C. Liu, K. Chiou, V. J. Wedeen, T. G. Reese, and C. Yang, "Diffusion tensor magnetic resonance imaging mapping the fiber architecture remodeling in human myocardium after infarction: Correlation with viability and wall motion," *Circulation*, vol. 114, no. 10, pp. 1036–1045, Aug. 2006.
- [30] J. D. Humphrey, *Cardiovascular Solid Mechanics: Cells, Tissues and Organs*. New York, NY, USA: Springer-Verlag, 2002.
- [31] P. J. Hunter, B. H. Smaill, P. M. F. Nielsen, and J. LeGrice, "Mathematical model of the cardiac anatomy," in *Computational Biology of the Heart*. New York, NY, USA: Wiley, ch. 6, 1996.
- [32] K. K. Nand, G. Hamarneh, and R. Abugarbieh, "Diffusion tensor image processing using biquaternions," in *Proc. 9th IEEE Int. Symp. Biomed. Imag.*, 2012, pp. 538–541.

Authors' photographs and biographies not available at the time of publication.